convective mixing from heat flow and thermohaline circulation simply destroys the molecular diffusion regime. But in the polar ice caps another effect intervenes: the accumulating firn acts like a giant columnar sieve through which the gravitational enrichment can be maintained by molecular diffusion undisturbed by convective motions. Positive enrichments of the isotopic and gas components that are less than the maximum predicted values probably represent significant variations in accumulation rates that determine the advective efflux of air from the firn back to the atmosphere, as well as with artifacts of analytical procedure when microfractures are present. Thus, 60 years after publication of the canonical theorem of Gibbs, a fluid system at the earth's surface—atmospheric gases in the firn layers of polar ice caps—has provided experimental verification of this effect (*19*).

REFERENCES AND NOTES

1. Y. Horibe, K. Shigehara, C. C. Langway, Jr., *Earth Planet. Sci. Lett.* **73**, 207 (1985).
2. M. Bender *et al.*, *Nature* **318**, 349 (1985).
3. T. A. Sowers, thesis, University of Rhode Island, Kingston (1987); T. Sowers, M. Bender, D. Raynaud, *J. Geophys. Res.*, in press.
4. H. Friedli *et al.*, *Nature* **324**, 237 (1986).
5. H. Craig, C. C. Chou, J. A. Welhan, C. M. Stevens, A. Engelkemeir, *Science* **242**, 1535 (1988).
6. The δ values, in per mil, $= 10^3 \cdot [(R/T_A) - 1]$ where R is the $^{18}O/^{16}O$ or $^{15}N/^{14}N$ ratio and R_A refers to the atmospheric ratio. We use δ for isotopic enrichments and Δ for enrichments of the molecular ratios O_2/N_2 and Ar/N_2.
7. At SIO gases were extracted from ~257-g ice samples by vacuum melting and cycled over hot carbon to convert O_2 to CO_2 as in (*1*). The remaining N_2-Ar fraction was input through I_2O_5 reagent (which totally removes CO) to our mass spectrometer for ^{15}N measurements. All samples were interspersed with standards containing the atmospheric N_2/Ar ratio. The methods used in the URI work are described in (*3*).
8. W. S. B. Paterson, *The Physics of Glaciers* (Pergamon Press, Oxford, ed. 2, 1981).
9. J. W. Gibbs, *Collected Works*, vol. 1, *Thermodynamics* (Yale Univ. Press, New Haven, 1928).
10. The firn density curve (7) was fit with an exponential from which the upward flux of air at any depth Z can be calculated as $(1/\rho_z - 1/\rho_t)$ times the ice accumulation rate, where ρ_t is the final density (0.83) at the firn to ice transition. The ratio of diffusive to advective gas fluxes can then be calculated approximately from the exponential concentration gradient: for N_2 this ratio varies from 0.16 at the surface, to 1 at $Z = 40$ m, to 24 at $Z = 68$ m, and is infinite at the transition layer. This ratio, and thus the accumulation rate, may be the controlling effect on scaling the effective isotopic enrichment relative to the calculated maximum value for zero advection. The advection velocity of gas varies from ~50 cm/year at the surface, to 1 cm/year at 65 m depth, and to 0 at the firn-ice interface.
11. D. Raynaud and J. M. Barnola, *Nature* **315**, 309 (1985).
12. R. C. Reid and T. K. Sherwood, *The Properties of Gases and Liquids* (McGraw-Hill, New York, ed. 2, 1966). The collision diameters are the Lennard-Jones potential values derived from viscosity data.
13. The effusion equation for Δ (or δ) is, in simplest form (no molecular interactions):

$$\Delta \sim [(M/M_i)^{0.5} - 1] \cdot 10^3 \cdot F_L \quad (3)$$

where F_L is the fraction of gas lost in the actual fractionating process. For ^{15}N the "single-stage enrichment" term is 17.3 per mil, which with a 2% loss of N_2 would give $\Delta = 0.35$ per mil.
14. In Eq. 1, it is assumed that gases in an element of firn continuously readjust to the time-independent equilibrium state as each element advects from the surface down to the firn-ice transition zone. The e-folding time for molecular diffusion over half the firn depth is $\sim(Z/2)^2/D$ (D is the diffusion coefficient in air), which is of the order of 1 year, during which time a firn element moves downward by ~0.5 to 0.02 m, so that this assumption is approximately true. A complete description of the gases in the firn column requires solutions of the diffusion equations in a porous medium with a moving boundary in a gravitational field, temperature gradients, coupling terms between diffusion coefficients of major components, vertical variation in the upward advection rate of gases (*10*), and the transient mixing effects of barometric pressure waves in the column. The barometric effects have a time scale of the order of weeks to months at the surface and are rapidly attenuated with depth by the decreasing porosity and increased resistance to gas flow, so that all these effects, the details of which are beyond the scope of this first paper, are expected to be of second order or less in importance.
15. H. Friedli, E. Moor, H. Oeschger, U. Siegenthaler, B. Stauffer, *Geophys. Res. Lett.* **11**, 1145 (1984).
16. L. D. Labeyrie, J. C. Duplessy, P. L. Blanc, *Nature* **327**, 477 (1987).
17. W. Dansgaard, *Deep Sea Res.* **6**, 346 (1960).
18. J. Mendelejev, *Dokl. Akad. Nauk SSSR* **3**, 105 (1935).
19. After completion of this paper and presentation as an A. L. Day lecture at Yale University, we learned that J. Schwander has discussed the possibility of gravitational effects on gas chemistry in firn [in *Proceeding of the Dahlen Workshop on the Environmental Record of Glaciers*, H. Oeschger and C. C. Langway, Jr., Eds. (Wiley, New York, in press)].

20. We thank D. Burtner and C. Nilson at SIO for dedicated assistance in the laboratory, M. Bender at URI for discussion, and V. K. Craig for the manuscript. H.C. thanks H. Ramberg for exciting his initial interest in gravitational thermodynamics. Work at SIO was supported by NSF grants DPP85-21486 and DPP87-22718; work at URI was supported by grant OCE85-01197 (M. Bender).

11 October 1988; accepted 9 November 1988

Restoration of Torque in Defective Flagellar Motors

DAVID F. BLAIR AND HOWARD C. BERG

Paralyzed motors of *motA* and *motB* point and deletion mutants of *Escherichia coli* were repaired by synthesis of wild-type protein. As found earlier with a point mutant of *motB*, torque was restored in a series of equally spaced steps. The size of the steps was the same for both MotA and MotB. Motors with one torque generator spent more time spinning counterclockwise than did motors with two or more generators. In deletion mutants, stepwise decreases in torque, rare in point mutants, were common. Several cells stopped accelerating after eight steps, suggesting that the maximum complement of torque generators is eight. Each generator appears to contain both MotA and MotB.

CELLS OF *Escherichia coli* AND MANY other motile bacteria swim by rotating helical flagellar filaments (*1, 2*). Each filament is driven at its base by a motor powered by the transmembrane proton gradient (*3*). The motor is only about 20 nm in diameter but is moderately complex, containing about 20 different polypeptides (*4*). Basal structures have been purified (*5, 6*) and shown by electron microscopy to consist of four rings (two in Gram-positive bacteria) mounted on a rod (*6, 7*). These basal structures are missing several proteins essential for torque generation (*8*), including MotA and MotB, which are both found in the cytoplasmic membrane (*9*). Mutants defective in MotA or MotB are paralyzed; their motors do not generate torque, even though the basal structures appear normal (*9, 10*). By inducing transcription of a wild-type *motB* gene carried on a plasmid in tethered cells of a *motB* missense mutant, Block and Berg (*11*) showed that restoration of torque takes place in a series of equal steps, indicating that MotB is a component in each of several independent torque generators. Here, we extend these studies to MotA as well as MotB, by use of deletion as well as missense mutants.

Cells of *motA* or *motB* strains were transformed with plasmids that carry *motA* or *motB* fused to the lactose promoter and $lacI^Q$ (an allele that overexpresses the structural gene for the *lac* repressor (*12*) (Table 1).

Table 1. Strains and plasmids.

Strain or plasmid	Relevant genotype
RP437	Wild type for motility and chemotaxis
MS5037	*motA*
RP3087	*motB 580*
RP6666	Δ*motA*
BL-19	Δ*motB1*
RP6894	Δ*motA*Δ*motB*
pDFB27	*para-motA*$^+$*motB*$^+$, *araC*$^+$, *Ap*^{R}
pDFB28	p*lac-motB*$^+$, *lacI*^{Q}, *Ap*^{R}
pDFB29	*para-motA*$^+$, *araC*$^+$, *Ap*^{R}
pDFB36	p*lac-motA*$^+$, *lacI*^{Q}, *Ap*^{R}
pSYC62	p*mocha-motB*$^+$, *Cm*^{R}

Department of Cellular and Developmental Biology, Harvard University, Cambridge, MA 02138, and the Rowland Institute for Science, Cambridge, MA 02142.

When tethered (*2*), these cells rotated very slowly or not at all. However, between 10 and 20 min after the addition of the *lac* inducer isopropyl β-D-thiogalactopyranoside (IPTG) (*13*), the cells began to rotate, increasing their speed over the course of several minutes. The stepwise increase in the clockwise (CW) and counterclockwise (CCW) speed of one such *motA* cell is shown in Fig. 1. The steps were of equal size, demonstrating the addition of equal torque increments. The close linear correlation between speed and level number is illustrated by additional examples (Fig. 1, inset).

Both CW and CCW rotation intervals were seen at all levels. Furthermore, the rotation speeds in the two directions were equal. This implies either that each torque generator can drive the motor with equal force in either direction, or that CW and CCW torque generators, if distinct ones exist, are always incorporated together. However, the cell shown in Fig. 1 spent a larger fraction of its time spinning CCW when at the lowest torque level than at higher levels. This behavior also was observed in the *motB* background (*11*).

The torque of a motor driving a tethered cell can be computed from the rotation speed, the viscosity of the medium, and the rotational and translational drag coefficients of the cell body (*14, 15*). The rotation speed can be measured by slow-speed playback of videotape records; the viscosity is known; and the drag coefficien can be calculated from the diameter, length, and radius of gyration of the image of the cell (*15, 16*). These measurements were made during resurrections of several *motA* and *motB* cells, and the torques for the lowest level were calculated. The results for the *motA* and *motB* cells were nearly the same (Table 2, rows 1 and 2). We also measured the torques in *motA* cells carrying pDFB36 (p*lac-motA*$^+$) cultured for 4 hours in the presence of 2.5 m*M* IPTG (Table 2, row 3), and in wild-type cells carrying pDFB27 (p*ara-motA*$^+$-*motB*$^+$) cultured for 4 hours in the presence of 0.2 m*M* arabinose (Table 2, row 4). The latter strain, which is expected to produce more MotA and MotB than the wild type containing no plasmid, had a torque comparable to that of the *motA* strain. Thus, the IPTG-induced *motA* strain (Table 2, row 3) was operating with at least as many torque generators as the strain containing excess MotA and MotB (Table 2, row 4). The mean torque for the IPTG-induced *motA* strain (Table 2, row 3) was approximately sevenfold that of the motors of the same strain operating at the lowest level (Table 2, row 1).

If we assume that the torque generators are independent and contribute equal torques, this ratio should reflect the number of torque generators in the complete motor. The larger values of 15 to 16 reported previously (*11*) were based on two types of measurements. (i) The mean speed of a population of wild-type cells was compared to the mean speed at the lowest level of a population of *motB* cells. Because the data for the two populations were drawn from separate experiments, it is possible that the populations had different characteristics, for example, protonmotive force, cell sizes, or tethering geometries. Rotational frictional drag coefficients increase nearly as the cube of the cell length. (ii) The maximum speed of a single resurrected cell was compared to

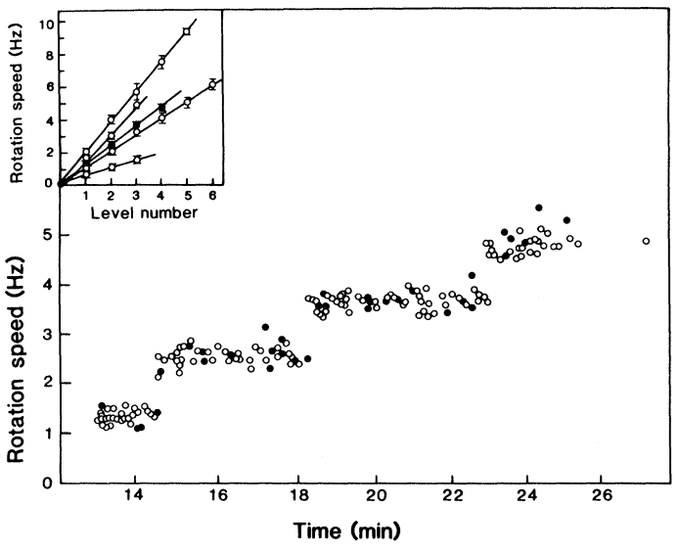

Fig. 1. Rotation speed of a tethered *motA* cell undergoing resurrection. Filled circles, clockwise; and open circles, counterclockwise. Cells of strain MS5037 (pDFB36) were cultured in tryptone broth containing ampicillin (50 μg/ml) to a density of approximately 5×10^8 cells per milliliter, then washed and tethered in motility medium as described (*24*). At 0 time, this medium was replaced with minimal salts medium containing 0.4% glycerol, 0.4% glucose, essential amino acids (1 m*M*), and 2.5 m*M* IPTG. Rotation speed was measured from videotapes played back at slow (1/8 or 1/16) speed; a stopwatch was used to time only those revolutions that contained no reversals. (Inset) Filled circles: the mean rotation speed of this cell at each level plotted as a function of the level number (±SEM for at least five measurements at each level). Open circles: similar data for four other cells of the same strain.

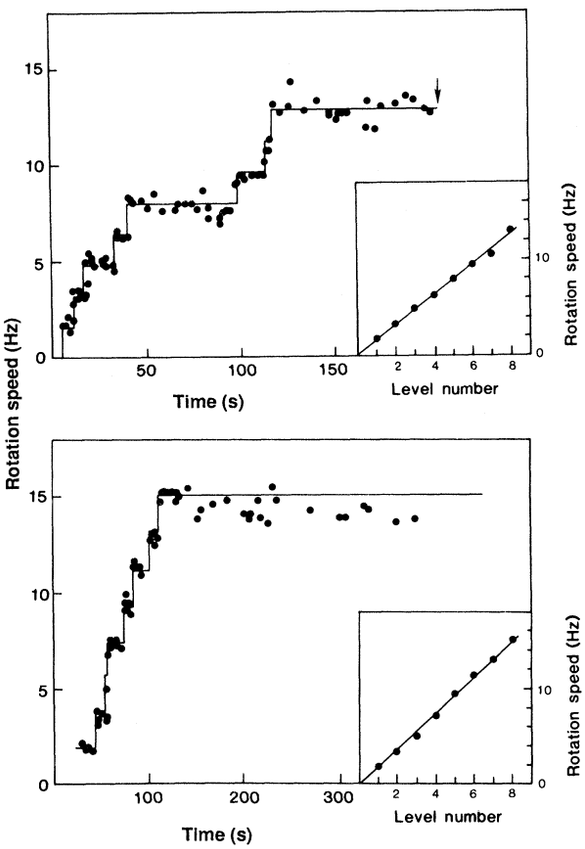

Fig. 2. Rotation speeds of two *motB* cells undergoing resurrection. Cells of strain RP3087 (pDFB28) were cultured in tryptone broth containing ampicillin (50 μg/ml) and washed and tethered in motility medium. Approximately 20 min before the periods shown, the medium was exchanged for a medium consisting of 90% motility medium, 10% tryptone broth, and 2.5 m*M* IPTG. The solid lines reflect the hypothesis that resurrection takes place in eight equal increments of speed. In the top panel, the arrow indicates when the cell fell off the cover slip. (Insets) Rotation speed versus level number for the corresponding cell.

its initial speed. We reexamined the videotape of this cell and found that it hesitated frequently at the lowest level, causing its speed at this level to be underestimated by the computer-based method used earlier (*11*). It also is possible that small changes in the tethering geometry with time reduced the drag on this cell at its maximum speed.

Our estimate of the number of torque generators, made on the basis of comparisons of cell populations, would be biased if cells with unusually high torques tended to fall off the cover slip. This possibility was ruled out by measuring the torques of a population of IPTG-induced *motA* cells (Table 2, row 3) over the course of more than 1 hour; no significant change in torque was observed [mean ± SEM at 7 min (37 cells), $12.4 \pm 0.5 \times 10^{-12}$ dyne-cm; at 32 min (29 cells), $12.6 \pm 0.5 \times 10^{-12}$ dyne-cm; and at 68 min (26 cells), $11.9 \pm 0.9 \times 10^{-12}$ dyne-cm].

The rates and yields of resurrections were substantially improved when resurrection was allowed to proceed in motility medium containing 10% tryptone broth (Fig. 2) instead of in minimal salts medium (Fig. 1). Many cells accelerated rapidly to a nearly constant speed. Among these, several were analyzed closely to resolve as many steps as possible. Two examples shown in Fig. 2 indicate that the motor contains at least eight torque generators. The resurrection plotted in the lower panel suggests that there are no more than eight; that cell stayed at the eighth level for a long time, eventually slowing down as it grew longer and its drag coefficient increased.

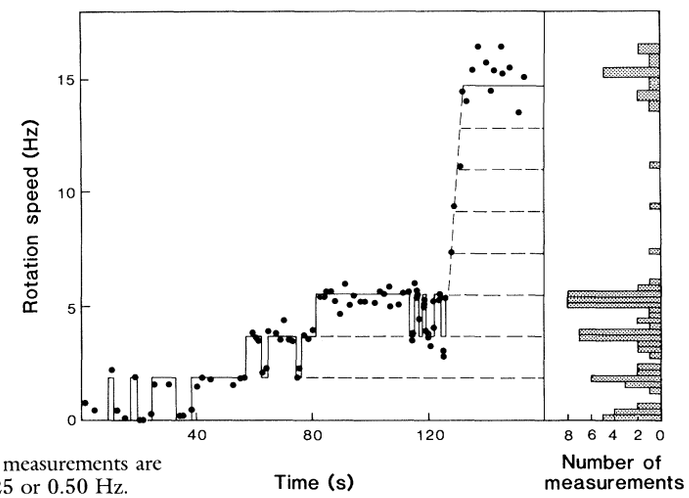

Fig. 3. Rotation speed of a tethered cell of a Δ*motB* strain undergoing resurrection. Cells of strain BL-19 (pDFB28) were cultured, tethered, and induced as described in Fig. 2, except that induction with IPTG took place approximately 10 min before the period shown. Rotation speed was sampled periodically, subject to the constraint that revolutions contained no reversals. The solid line was drawn as in Fig. 2. Dashed lines indicate torque levels. In the histogram, the speed measurements are binned in intervals of 0.25 or 0.50 Hz.

Table 2. Torques of *E. coli* flagellar motors. Torques were computed by using video images to estimate cell sizes. One culture of RP437 (pDFB27) was grown in the presence of 0.2 m*M* arabinose and tethered, and the cell sizes were estimated both from video images and photomicrographs. The estimates of average torque obtained by these two methods were the same, indicating that blooming of the video images did not exaggerate the sizes of the cells. Overnight cultures were diluted 100-fold, grown for 4 hours in tryptone broth without IPTG (rows 1 and 2) or with 2.5 m*M* IPTG (row 3) or 0.2 m*M* arabinose (row 4), and tethered in motility medium. Resurrections of tethered cells (rows 1 and 2) were carried out by adding 2.5 m*M* IPTG in motility medium supplemented with 10% tryptone broth. Motors were considered to contain a single torque generator if they started spinning during the experiment and showed rotational Brownian motion to indicate that they were not tightly stuck to the cover slip before starting, or if they were spinning initially at a speed that later increased in simple multiples. The torques of cells selected by these two criteria were the same.

Strain	Inducer	MotA, MotB complement	Torque (mean ± SEM, 10^{-12} dyne-cm)	Number of cells
MS5037 (pDFB36)	2.5 m*M* IPTG	MotA at lowest level	1.91 ± 0.07	68
RP3087 (pDFB28)	2.5 m*M* IPTG	MotB at lowest level	1.78 ± 0.12	26
MS5037 (pDFB36)	2.5 m*M* IPTG	MotA in excess	13.0 ± 0.5	136
RP437 (pDFB27)	0.2 m*M* arabinose	MotA, MotB in excess	12.2 ± 0.5	56
RP437	None	MotA, MotB at wild-type levels	8.8 ± 0.64	13
RP437 (pDFB27)	None	MotA, MotB at slight excess of wild-type levels	10.5 ± 0.67	26

The time course of resurrection of a strain carrying a deletion (Δ*motB*) is shown in Fig. 3. In contrast to the resurrections of the point mutants, rapid fluctuations of torque were observed: decreases in torque after resurrection to a given level, rare in the point mutants, occurred frequently. Steps up and down were of equal size. In accelerating to its final speed, this cell went from level 2 to level 8 in approximately 7 s (Fig. 3). Similar results were seen in resurrections in a Δ*motA* background, with the use of strain RP6894 (Δ*motA*Δ*motB*) containing pSYC62 (p*mocha-motB*$^+$) to restore MotB and pDFB36 (p*lac-motA*$^+$) to permit controlled introduction of MotA. These results suggest that in the point mutants, defective copies of the Mot proteins are present in the motor before resurrection. During resurrection, they delay the incorporation of functional copies, but stabilize their association with the motor once the copies are incorporated.

If defective copies of MotA compete with functional copies, then the population comparisons of Table 2 underestimate the number of torque generators in a fully functional motor, because both kinds of copies are present in the fully induced cell. A correction for this effect can be made if it is assumed that the replacement of mutant MotA protein by wild-type MotA protein is adequately described in terms of competitive binding to a limited number of sites on the motor. Presumably, such competition occurs in a wild-type cell, where the number of copies of MotA exceeds the number of available sites (*17*). The average motor torque was found to increase hyperbolically with increasing concentration of IPTG in a culture of MS5037 (pDFB36), with half-maximal torque at 25 μ*M* IPTG (*18*). Based on assays of β-galactosidase activity in another strain carrying *lacI*^{Q}, the maximum level of expression from the *lac* promoter was about seven times larger than the level at 25 μ*M* IPTG (*19*). If these numbers are used to correct the torques in Table 2, the estimate of the number of torque generators in a fully functional motor increases from 6.8 to 8.2.

The torques for the wild-type strain and for the wild-type strain containing pDFB27 not induced with arabinose were only 4.6 and 5.5 times larger, respectively, than those of the one-generator motors (Table 2). These results suggest that the average wild-type cell harvested in exponential phase does not possess a full complement of torque generators. Khan *et al.* (*20*) have shown that cytoplasmic membranes of flagellated strains of *E. coli* contain rings of between 10 and 12 particles. These rings were not found if either of the Mot proteins was absent. Rings of particles also were seen in *Streptococcus*,

except that each ring contained between 14 and 16 particles. Coulton and Murray saw rings of between 14 and 16 particles surrounding annular depressions in membranes at the poles of *Aquaspirillum serpens* (*21*). Taken together, these results suggest that the number of particles in a fully functional *E. coli* motor might be as high as 16. If so, our results would indicate that there are two particles per force generator.

The amino acid sequences of MotA and MotB have been determined from the nucleotide sequences of their genes (*22*). MotB is moderately hydrophobic, and MotA is significantly more so. The MotA sequence contains four strongly hydrophobic segments that are probably transmembrane α helices; the MotB sequence has only one. By using Tn*phoA* insertions into *motB* and controlled proteolysis of MotB, Chun and Parkinson (*23*) have shown that MotB traverses the cytoplasmic membrane once near its NH_2-terminus, with its bulk situated in the periplasm. They suggest that MotB could serve as a linker that connects the torque-generating machinery of the motor to the cell wall. MotA topology has not yet been examined as closely, but its four hydrophobic segments together contain enough moderately polar, hydrogen-bonding residues (for example, Ser, Thr, Asn, and His) to enable them to form a proton-conducting channel. If so, each pair of membrane particles, and each force generator, might comprise one or more MotB linkers and MotA channels.

REFERENCES AND NOTES

1. H. C. Berg and R. A. Anderson, *Nature* **245**, 380 (1973).
2. M. Silverman and M. Simon, *ibid.* **249**, 73 (1974).
3. S. H. Larsen *et al.*, *Proc. Natl. Acad. Sci. U.S.A.* **71**, 1239 (1974); T. N. Belyakova, A. N. Glagolev, V. P. Skulachev, *Biochemistry USSR* **41**, 1206 (1976); H. C. Berg, M. D. Manson, M. P. Conley, *Symp. Soc. Exp. Biol.* **35**, 1 (1982).
4. The purified basal structure contains some 15 different polypeptides, but the intact motor is likely to contain, in addition, the products of the *flaAII, flaBII, motD, motA*, and *motB* genes (*8*).
5. M. L. DePamphilis and J. Adler, *J. Bacteriol.* **105**, 376 (1971).
6. S.-I. Aizawa *et al.*, *ibid.* **161**, 836 (1985).
7. M. L. DePamphilis and J. Adler, *ibid.* **105**, 384 (1971).
8. R. M. Macnab, in Escherichia coli *and* Salmonella typhimurium: *Cellular and Molecular Biology*, F. C. Neidhardt *et al.*, Eds. (American Society for Microbiology, Washington, DC, 1987), pp. 70–83; S. Yamaguchi *et al.*, *J. Bacteriol.* **168**, 1172 (1986).
9. M. Silverman, P. Matsumura, M. Simon, *Proc. Natl. Acad. Sci. U.S.A.* **73**, 3126 (1976).
10. J. B. Armstrong and J. Adler, *Genetics* **56**, 363 (1967); M. Hilmen and M. Simon, in *Cell Motility*, R. Goldman, T. Pollard, J. Rosenbaum, Eds. (Cold Spring Harbor Laboratory, Cold Spring Harbor, NY, 1976), pp. 35–45.
11. S. M. Block and H. C. Berg, *Nature* **309**, 470 (1984).
12. B. Müller-Hill, L. Crapo, W. Gilbert, *Proc. Natl. Acad. Sci. U.S.A.* **59**, 1259 (1968).
13. W. Gilbert and B. Müller-Hill, *ibid.* **56**, 1891 (1966).
14. H. C. Berg, *Nature* **249**, 77 (1974).
15. M. Meister and H. C. Berg, *Biophys. J.* **52**, 413 (1987).
16. M. M. Tirado and J. G. de la Torre, *J. Chem. Phys.* **71**, 2581 (1979); *ibid.* **73**, 1986 (1980).
17. M. L. Wilson and R. M. Macnab, *J. Bacteriol.* **170**, 588 (1988).
18. D. F. Blair and H. C. Berg, unpublished results.
19. K. A. Fahrner and H. C. Berg, unpublished results.
20. S. Khan *et al.*, *J. Mol. Biol.* **202**, 575 (1988).
21. J. W. Coulton and R. G. E. Murray, *J. Bacteriol.* **136**, 1037 (1978).
22. G. E. Dean, R. M. Macnab, J. Stader, P. Matsumura, C. Burks, *ibid.* **159**, 991 (1984); J. Stader, P. Matsumura, D. Vacante, G. E. Dean, R. M. Macnab, *ibid.* **166**, 244 (1986).
23. S. Y. Chun and J. S. Parkinson, *Science* **239**, 276 (1988).
24. S. M. Block *et al.*, *J. Bacteriol.* **154**, 312 (1983).

25. We thank M. D. Manson for strain BL-19; J. S. Parkinson for strains RP437, RP3087, RP6666, and RP6894; M. I. Simon for strain MS5037; and S. Y. Chun for plasmid pSYC62. We also thank S. M. Block and D. Fung for comments on the manuscript, and K. A. Fahrner for assays of β-galactosidase activity. Supported by NSF grant DMB-8645909. D.F.B. began this work as a Public Health Service postdoctoral fellow (AI07456) and is currently a Burroughs Wellcome Fund fellow of the Life Sciences Research Foundation.

5 July 1988; accepted 17 October 1988

Association of Transfer RNA Acceptor Identity with a Helical Irregularity

WILLIAM H. MCCLAIN, YONG-MIN CHEN, K. FOSS, JAY SCHNEIDER

The aminoacylation specificity ("acceptor identity") of transfer RNAs (tRNAs) has previously been associated with the position of particular nucleotides, as opposed to distinctive elements of three-dimensional structure. The contribution of a G·U wobble pair in the acceptor helix of $tRNA^{Ala}$ to acceptor identity was examined with synthetic amber suppressor tRNAs in *Escherichia coli*. The acceptor identity was not affected by replacing the G·U wobble pair in $tRNA^{Ala}$ with a G·A, C·A, or U·U wobble pair. Furthermore, a $tRNA^{Ala}$ acceptor identity was conferred on $tRNA^{Lys}$ when the same site in the acceptor helix was replaced with any of several wobble pairs. Additional data with $tRNA^{Ala}$ show that a substantial acceptor identity was retained when the G·U wobble pair was translocated to another site in the acceptor helix. These results suggest that the G·U wobble pair induces an irregularity in the acceptor helix of $tRNA^{Ala}$ to match a complementary structure in the aminoacylating enzyme.

THE ACCEPTOR IDENTITY OF *ESCHERICHIA COLI* $tRNA^{Ala}$ is partially determined by a G·U wobble pair in the acceptor stem of the molecule. The acceptor stem is helical, and this structural feature is generally assumed to be common to all tRNAs. The importance of this G·U wobble pair to $tRNA^{Ala}$ acceptor identity was initially suggested in biochemical and genetic experiments (*1*), and was eventually established by replacing the wild-type base pair in other tRNAs with a G·U wobble pair and observing acceptor identity changing to $tRNA^{Ala}$ (*2, 3*). The wobble pairing between G and U displaces these bases relative to those of Watson-Crick pairs, giving the grooves of the helix a distinctive pattern of functional groups (*4*). The available data indicate that the G·U wobble pair is incor-

Department of Bacteriology, University of Wisconsin, Madison, WI 53706.

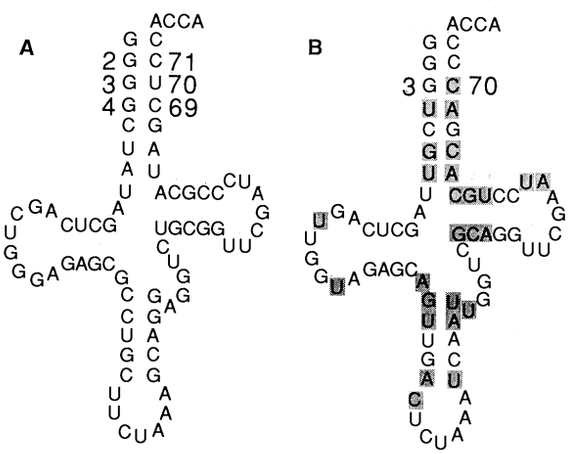

Fig. 1. Nucleotide sequence of the amber suppressors of (**A**) $tRNA^{Ala}$ (*2*) and (**B**) $tRNA^{Lys}$ (*8*). Numbers identify base pair positions in the acceptor helix. Shaded nucleotides in $tRNA^{Lys}$ differ from those in $tRNA^{Ala}$.